



HAL
open science

Infrasound From Large Earthquakes Recorded on a Network of Balloons in the Stratosphere

Raphael F. Garcia, Adrien Klotz, Albert Hertzog, Roland Martin, Solène G erier, Ervan Kassarian, J er me Bordereau, St ephanie Venel, David Mimoun

► **To cite this version:**

Raphael F. Garcia, Adrien Klotz, Albert Hertzog, Roland Martin, Sol ene G erier, et al.. Infrasound From Large Earthquakes Recorded on a Network of Balloons in the Stratosphere. *Geophysical Research Letters*, 2022, 49, 10.1029/2022GL098844 . insu-03778095

HAL Id: insu-03778095

<https://insu.hal.science/insu-03778095>

Submitted on 15 Sep 2022

HAL is a multi-disciplinary open access archive for the deposit and dissemination of scientific research documents, whether they are published or not. The documents may come from teaching and research institutions in France or abroad, or from public or private research centers.

L'archive ouverte pluridisciplinaire **HAL**, est destin ee au d ep ot et  a la diffusion de documents scientifiques de niveau recherche, publi es ou non,  emanant des  tablissements d'enseignement et de recherche fran ais ou  trangers, des laboratoires publics ou priv es.



Distributed under a Creative Commons Attribution 4.0 International License

Geophysical Research Letters[®]



RESEARCH LETTER

10.1029/2022GL098844

Key Points:

- An earthquake is detected by a network of barometers on board balloons in the stratosphere for the first time
- Quake magnitude and distance are estimated from the infrasound created by seismic body waves and surface waves
- Balloons can act as mobile seismometer network in the atmosphere of Earth and Venus

Supporting Information:

Supporting Information may be found in the online version of this article.

Correspondence to:

R. F. Garcia,
raphael.garcia@isac.fr

Citation:

Garcia, R. F., Klotz, A., Hertzog, A., Martin, R., G erier, S., Kassarian, E., et al. (2022). Infrasound from large earthquakes recorded on a network of balloons in the stratosphere. *Geophysical Research Letters*, 49, e2022GL098844. <https://doi.org/10.1029/2022GL098844>

Received 29 MAR 2022

Accepted 4 JUL 2022

Author Contributions:

Conceptualization: Raphael F. Garcia, David Mimoun

Data curation: Adrien Klotz, J r me Bordereau

Formal analysis: Raphael F. Garcia, Albert Hertzog

Funding acquisition: Raphael F. Garcia, David Mimoun

Investigation: Roland Martin, Sol ne G erier, Ervan Kassarian

Methodology: Raphael F. Garcia

Project Administration: Raphael F. Garcia, St phanie Venel

Resources: Albert Hertzog, J r me Bordereau

  2022. The Authors.

This is an open access article under the terms of the [Creative Commons Attribution License](https://creativecommons.org/licenses/by/4.0/), which permits use, distribution and reproduction in any medium, provided the original work is properly cited.

Infrasound From Large Earthquakes Recorded on a Network of Balloons in the Stratosphere

Raphael F. Garcia¹ , Adrien Klotz¹ , Albert Hertzog², Roland Martin³, Sol ne G erier¹, Ervan Kassarian¹, J r me Bordereau^{2,4}, St phanie Venel⁴, and David Mimoun¹ 

¹Institut Sup rieur de l'A ronautique et de l'Espace (ISAE-SUPAERO), Universit  de Toulouse, Toulouse, France,

²Laboratoire de M t orologie Dynamique / Institut Pierre-Simon Laplace (LMD/IPSL), Sorbonne Universit ,  cole Polytechnique,  cole Normale Sup rieure (ENS), Centre National de la Recherche Scientifique (CNRS), Paris, France,

³G oscience Environnement Toulouse, Observatoire Midi-Pyr n es, Universit  de Toulouse, Toulouse, France, ⁴Centre National d' tudes Spatiales, Toulouse, France

Abstract The ground movements induced by seismic waves create acoustic waves propagating upward in the atmosphere, thus providing a practical solution to perform remote sensing of planetary interiors. However, a terrestrial demonstration of a seismic network based on balloon-carried pressure sensors has not been provided. Here we present the first detection of seismic infrasound from a large magnitude quake on a balloon network. We demonstrate that quake's properties and planet's internal structure can be probed from balloon-borne pressure records alone because these are generated by the ground movements at the planet surface below the balloon. Various seismic waves are identified, thus allowing us to infer the quake magnitude and location, as well as planetary internal structure. The mechanical resonances of balloon system are also observed. This study demonstrates the interest of planetary geophysical mission concepts based on seismic remote sensing with balloon platforms, and their interest to complement terrestrial seismic networks.

Plain Language Summary After a quake, the surface of our planet vibrates like the surface of a drum. These vibrations generate sound waves at low frequencies that propagate upward in the atmosphere. These signals from two earthquakes have been recorded by barometers on board a network of long duration high altitude balloons deployed by the Strateole-2 experiment. The analysis of these records demonstrates that the amplitude and arrival time of the vibrations are properly predicted by our modeling tools. The oscillations of the balloon/gondola system forced by the acoustic waves are also observed, but the quake distance and magnitude can be estimated only from the data recorded on board the balloon gondolas. Moreover, the shape of the pressure perturbations recorded by the balloons contains the seismic surface waves that are sounding the first hundred kilometers of the Earth's internal structure. These observations clearly demonstrate the interest of a similar experiment in the atmosphere of Venus to sound its poorly known internal structure.

1. Introduction

The acoustic and gravity waves created by quakes can be used to constrain the seismic source mechanism and the planetary interior, as well as to infer the capability of quakes to produce tsunamis (Astafyeva, 2019). These atmospheric waves are also critical to infer the internal structure of planets with dense and hot atmospheres, like Venus, for which the surface deployment of a seismometer is very challenging (Garcia et al., 2005; Stevenson et al., 2015). These signals were first inferred from their induced variations of electron content in the ionosphere and atmospheric airglow emissions by remote sensing methods (Hines, 1960; Lognonn  et al., 2006). Then, in situ measurements based on satellite drag variations were described (Garcia et al., 2013, 2014). Quake signal observations from pressure sensors on board balloons have been studied recently in order to validate mission concepts for future Venus exploration (Bowman & Krishnamoorthy, 2021; Garcia et al., 2020; Krishnamoorthy et al., 2019). However an observation of a natural quake event with a realistic geometry was still missing to fully validate the observational concept and the amplitude scaling laws. After a first detection of a local quake of small magnitude by a pressure sensor on a stratospheric balloon (Brissaud et al., 2021), we present here the first detection of a quake by a network of pressure sensors in the stratosphere on board Strateole-2 balloons.

Software: Adrien Klotz, Roland Martin, Ervan Kassarian

Validation: Adrien Klotz, Albert Hertzog

Visualization: Raphael F. Garcia, Adrien Klotz

Writing – original draft: Raphael F. Garcia, Adrien Klotz, Albert Hertzog, Roland Martin, Solène G erier

Writing – review & editing: Sol ene G erier, St ephane Venel, David Mimoun

2. Strateole-2 Pressure Data

Strateole-2 project is an international project led by Centre National d’Etudes Spatiales (CNES). It deploys long-duration super-pressure balloons in the lower stratosphere, between 18 and 20 km altitude, in order to study troposphere-stratosphere coupling in the tropical atmosphere (Haase et al., 2018). The balloons are released from Mah  Island, Seychelles (5 S) and then drift close to the equator following stratospheric winds. The project is organized into three distinct campaigns, and the present study uses observations performed during the second campaign, in fall 2021.

Each of the 16 balloon flights carries the EUROS gondola which is in charge of the flight safety. This gondola includes a Global Positioning System (GPS) receiver (U-block) and the Temperature Sensor (TSEN) instrument (Podglajen et al., 2014) which is composed of temperature sensors and a Paroscientific pressure sensor model 6000-15A. The gondola position from GPS is provided every 30 s with a typical noise level of about 1 m. The pressure sensor in Nano-resolution mode provides absolute pressure measurements every second with a resolution around 1 μPa and a flat response up to our Nyquist frequency of 0.5 Hz, except for a low pass anti-aliasing filter of 0.35 Hz corner frequency which is corrected in our spectral estimates. Figure 2a presents the background pressure signal computed by using pwelch method in a 1 hour window before the events considered here. This signal, labeled “Noise” in Figure 2a, does not come from the sensor noise level (below $1 \text{ mPa}/\sqrt{\text{Hz}}$ in the 0.01–1 Hz frequency range), but mainly from external contributions such as balloon movements in the atmospheric pressure gradient and induced air flows, possibly enhanced by the lack of a dedicated inlet. At frequencies higher than the one of the neutral balloon oscillations (Vincent & Hertzog, 2014) ($\sim 4 - 5 \times 10^{-3}$ Hz), the background pressure signal decreases with frequency, until an energy peak is found around 0.2 Hz, the so called micro-baroms (Bowman & Lees, 2018), associated with interfering ocean waves (Figure 2).

Two quakes of magnitude larger than 7 occurred during the second Strateole-2 campaign, with balloons within 3,000 km from the quake source locations (Table 1). For the Earthquake in Northern Peru, a single balloon at 937 km distance detected a significant signal (Figure S2 in Supporting Information S1). For the Earthquake in Flores sea, four balloons within 3,000 km distance detected signals above background noise in the 0.05–0.5 Hz frequency range after the quake (Figure 1). Our study will focus on the quake in Flores sea. Unfortunately, 60 s of data are missing from 03:30:08 GMT to 03:31:07 GMT at the beginning of the main signal on balloon flight ST2_C1_16_TTL5.

During these events, the average balloon horizontal velocity was in between 4 m/s and 10 m/s. This speed is much smaller than both seismic surface wave speed (4 km/s) and sound speed (0.35 km/s). In addition, the maximum horizontal displacement during the 10 min of quake related signal is 6 km, which is much smaller than the seismic surface wave wavelength at 10-s period (40 km). Along the vertical direction, the balloons are oscillating at a period of 4.68×10^{-3} Hz with an amplitude of about 140 m. As a consequence, the balloons can be considered as point measurements at a given location for the physical processes considered here.

3. Validation of Observed Quake Signals

The signals observed on the four stratospheric balloons close to the Flores sea quake have arrival times consistent with acoustic signals generated by the ground movements induced by the seismic waves (Figure 3). In addition, these signals can be simulated by the upward propagation of pressure perturbations computed from the ground vertical-velocity forcing extracted from seismometer recordings below the balloon positions (Figures 3a and 3c) (Garcia et al., 2013; Martire et al., 2018, 2022; Waxler & Assink, 2019). In the time range considered here we do not expect to observe acoustic waves coming from the epicenter area, but just acoustic waves created by seismic waves below the balloon. Due to the low attenuation of acoustic waves below 1 Hz during the upward propagation, the effect of the atmosphere is simply a multiplication by a factor ≈ 0.3 , due to impedance contrast between ground and balloon altitude, and a time delay taking into account the propagation time of acoustic waves between the ground and the balloon altitude (≈ 60 s for a balloon at 18.7 km altitude). This simulation demonstrates that the balloon pressure record and the vertical velocity of the ground have similar spectral shapes. This spectral shape is consistent with the earthquake source model with a source cut-off frequency in the 0.04–0.1 Hz band, as expected for quakes of this magnitude (Ekstr m et al., 2012).

Table 1
Centroid Quake Parameters Extracted From GLOBALCMT Data Base

	Origin time	Latitude	Longitude	Depth	Mw	Ms	Source half
	(GMT)	(degree N)	(degree E)	(km)			duration (s)
Northern Peru	2021/11/28 10:52:25.8	-4.73	-76.74	110.3	7.5	7.5	13.4
Flores Sea	2021/12/14 03:20:35.8	-7.45	121.97	14.4	7.3	7.3	11.4

However, the observed pressure perturbations are larger than predicted by our simulations of upward propagation of ground motions in the 0.06–0.15 Hz frequency range. As observed in panels 2.a, 3.a and 3.c this over-amplification is peaking at a frequency of ~70 mHz in the records of both balloon 16 and 17 records. Additional over-amplified frequency peaks are also observed in these balloon-borne pressure records of the infrasounds created by the seismic waves. Because these resonances are not observed on ground records of vertical ground velocity, we investigated various potential sources for these signals. First, we reject potential reflections of acoustic waves in atmosphere layers because the almost vertical incidence of the incoming acoustic wavefield would require very steep changes of acoustic impedance, and so atmospheric properties, in order to trap such waves.

Then, the pendulum oscillation modes were modeled by using the method developed by Kassarian et al. (2021) (Text S1 and Table S2 in Supporting Information S1). The outputs of this model (Figure S1 in Supporting Information S1) demonstrate that no pendulum oscillation modes are expected below 0.1 Hz. In addition, the effect of gondola oscillations is a second order effect on the altitude of the gondola and consequently on the measured pressure variations. The observed pressure variations around 70 mHz (1.2 and 0.3 Pa peak to peak in records of balloons 17 and 16, respectively) imply vertical oscillations of the pressure sensor of 92 and 22 cm, if these variations were only due to the balloon vertical dynamics. However, due to a second order dependency on oscillation angle these values would imply oscillation amplitudes of respectively 22° and 11° for balloons 17 and 16. These numbers are much larger than the ones expected for such balloon systems, thus excluding fully the interpretation of this resonance in terms of gondola oscillations.

The vertical oscillations of the mass/spring system formed by the gondola/flight train attached to the balloon were furthermore considered. However, the spring lengths being on the order of 10 m, oscillations of 92 cm would imply a spring length variation of more than 9% which is unrealistic for a forcing by an acoustic wave of less than 1 Pa amplitude.

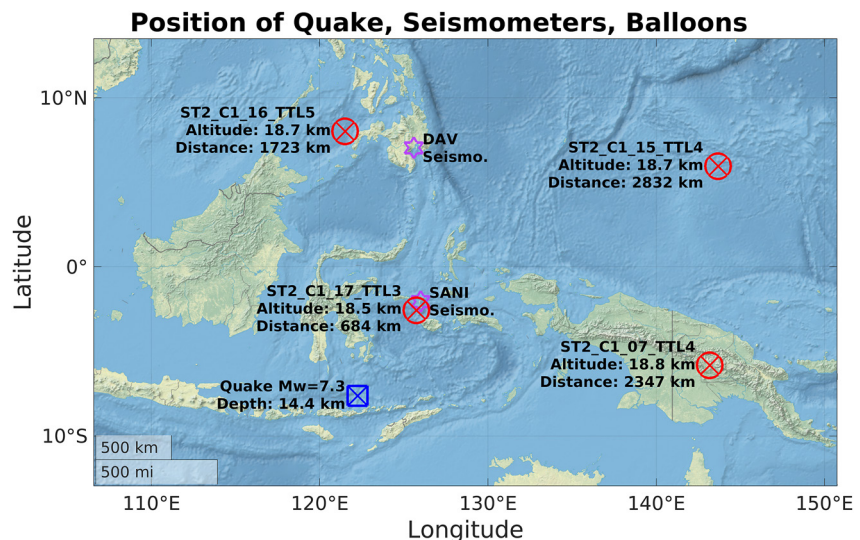


Figure 1. Position of the quake in Flores Sea (Blue square), the ground seismometers (purple stars) and Strateole-2 balloons (red circles) during the event. Balloon names, altitude and horizontal distance to the quake are also provided.

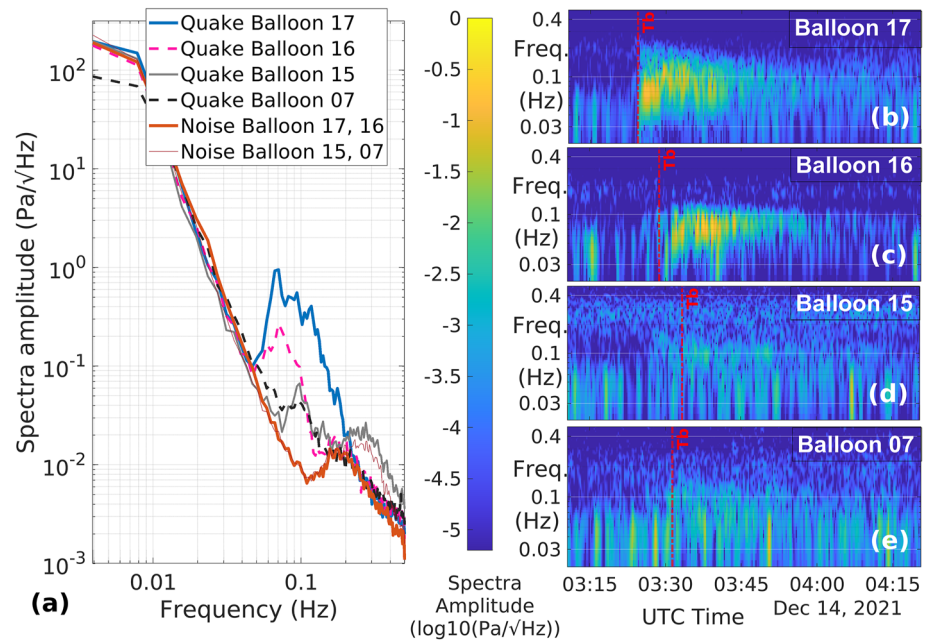


Figure 2. Spectra and spectrograms of the pressure records by Strateole-2 balloons. (a) Amplitude spectral density of the pressure records of the quake by the different balloons (blue, pink, gray and black curves) and background noise (red/brown curves). On the left (b–e), spectrograms of the pressure records after the quake in the 0.03–0.5 Hz frequency range. A time window of 35 s with a 70% overlap is used for the spectrogram computation, thus providing a frequency resolution of 0.0286 Hz. The red vertical dashed lines are indicating the theoretical arrival time of first arrival acoustic waves on the different balloons. A 1 min data gap is present on balloon 16 starting at 03:30:08 UTC.

Finally, we considered the excitation of the harmonics of the balloon neutral buoyancy frequency by the acoustic wave forcing. An analysis of the spectrum of the time derivative of pressure records with a better frequency resolution (Figure S3 in Supporting Information S1) demonstrates that the resonances observed during the quake are multiples of the balloon neutral buoyancy frequency. This observation suggests that the air pressure, air density and air velocity variations of the acoustic waves forced the vertical oscillations of the balloon in the frequency range of the main seismic signals (60–85 mHz), and so excited the harmonics of the balloon neutral buoyancy frequency. As a consequence, the observed pressure variations are dominated by the induced vertical movements of the balloon. The development of the physical model of the balloon vertical forcing by acoustic waves is beyond the scope of this paper, but our observations suggest that such a model is necessary for a full understanding of these data.

The time domain comparisons between the pressure records at the balloon altitudes and those deduced from seismometers are presented in Figures 3b and 3d. This demonstrates that acoustic waves generated by seismic S body wave and Rayleigh seismic surface waves can be identified, and that their relative arrival time are identical to those observed on the ground below the balloon.

This event is also a unique opportunity to test our scaling relations of infrasound amplitude with quake surface-wave magnitude and distance to the quake. The relation between (a) the amplitude of the ground displacement with a 20-s period and (b) the surface wave magnitude and distance to quake is derived from an empirical model (Mutschlechner & Whitaker, 2005). This ground displacement with a 20-s period is converted into ground velocity with a 10-s period assuming a flat displacement source spectrum in this period range. From the specific acoustic impedance (Salomons, 2001) at the interface between the ground and the atmosphere, we obtain the pressure perturbation at ground level at 10-s period:

$$\Delta_{\max} P_0 = A_v \rho_0 c_0 \quad (1)$$

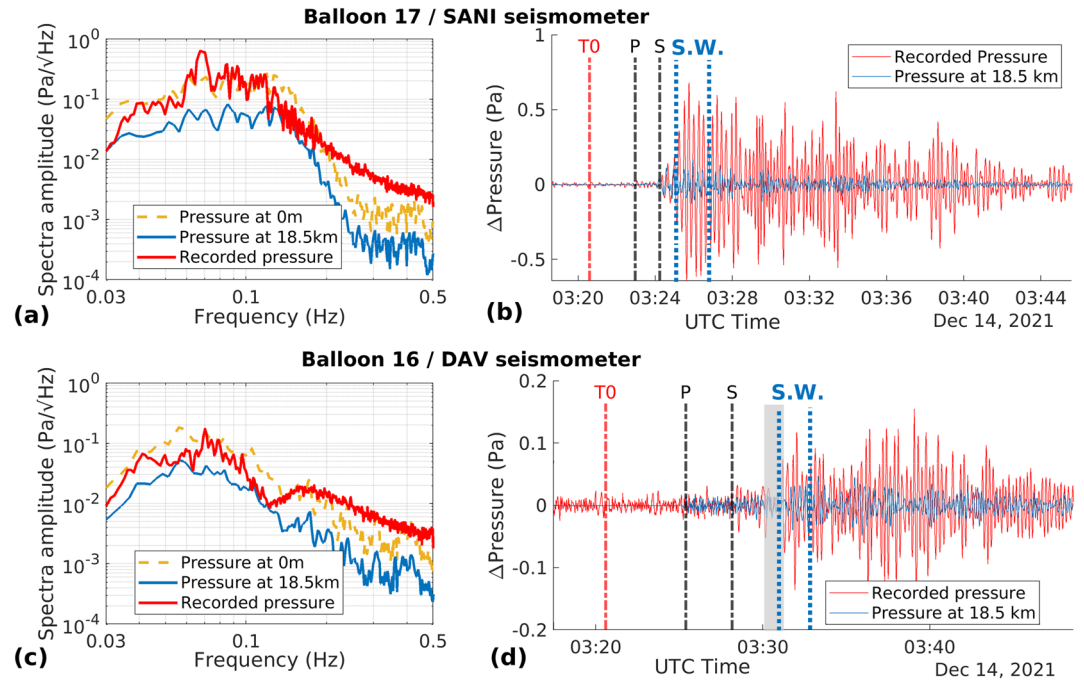


Figure 3. Comparison between pressure records and upward propagation of pressure perturbations induced by the ground vertical velocity. Spectra (a and c) and time domain pressure perturbations (b and d) are provided for Balloon 17 compared to SANI seismometer records (a and b), and for Balloon 16 compared to DAV seismometer records (c and d). The waveforms presented in this figure are band pass filtered in the 0.03–0.5 Hz frequency range. Origin time of the quake, and theoretical arrival times of pressure perturbations generated by P, S and Rayleigh Surface Waves (S.W.) at balloon altitude are provided as vertical dashed lines. A 1 min data gap is present on balloon 16 starting at 03:30:08 UTC. It is indicated by the gray shading area.

where A_v is the ground velocity deduced from surface wave magnitude, ρ_0 and c_0 are respectively the atmospheric density and the speed of sound at ground level. Assuming a low attenuation of the sound waves with 10-s periods, we predict the pressure perturbation at balloon altitude z from the acoustic impedance ratio, that is:

$$\Delta_{\max} P(z) = \Delta_{\max} P_0 \sqrt{\frac{\rho(z)c(z)}{\rho_0 c_0}} \quad (2)$$

with $\rho(z)$ and $c(z)$ respectively the density and sound speed at balloon altitude. These simple predictions are compared to the maximum pressure perturbations recorded by the 4 Strateole-2 balloons in the 0.085–0.125 Hz range in Figure 4a. The Strateole-2 pressure data demonstrate that these scaling relations are verified, except for Balloon 07 which is in the direction of a minimum of seismic surface-wave radiation by the quake.

The records of the event occurring in Northern Peru are presented in Figure S2 in Supporting Information S1. While being an event of similar magnitude as the one described previously, the dominant frequency of the quake signal is significantly higher (≈ 0.23 Hz). This observation suggests that either the acoustic wave radiation is either due to seismic waves interacting with the surface topography of the closeby Andes mountains (Martire et al., 2022; Pichon et al., 2006), or because of ground resonances in the amazonian basin below the balloon (Marchetti et al., 2016; Shani-Kadmiel et al., 2018). Further investigations are needed to properly decipher between these two effects.

4. Testing an Analysis of Venus Like Observations

In order to infer the capability of such balloon-borne observations to recover the seismic source and internal structure for planetary applications, we now analyze the data assuming that these parameters are not known.

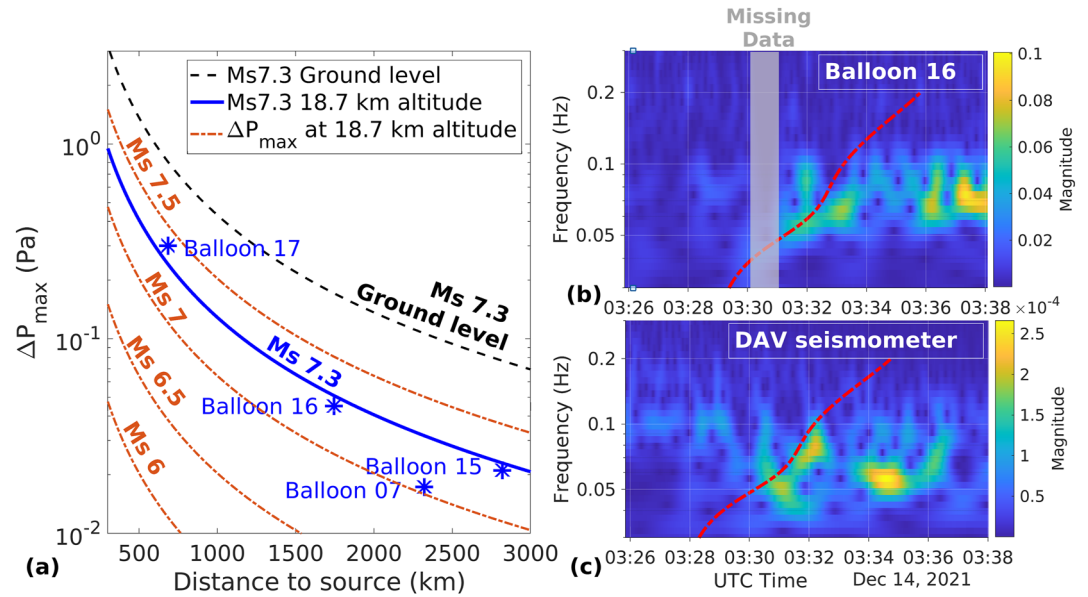


Figure 4. (a) Maximum pressure perturbation (Pa) at 18.7 km altitude and 10 s period as a function of horizontal distance to the quake (km) for different surface wave magnitudes (Ms) of the quake. Dashed red lines and blue line are theoretical computations at 18.7 km altitude. Black dashed line is the theoretical computation at ground level. Blue stars are measured values on pressure records of Strateole-2 balloons after band pass filtering in the 0.085–0.125 Hz range. Scalograms of pressure records of balloon 16 (b) and vertical component of seismometer DAV (c) computed with a continuous wavelet transform using the Morse wavelet. Theoretical surface wave arrival times are computed from group velocity dispersion curves using the internal structure model of Table S1 in Supporting Information S1 and shown as thick dashed red lines. For balloon data these arrival times are predicted with quake distance and origin time deduced from balloon data only, whereas for the DAV seismometer these are computed with quake parameters in Table 1. Note the 60 s time shift between the two dispersion curves induced by the propagation time of acoustic waves from the ground (c) to the balloon altitude (b).

First the quake cutoff frequency is estimated from the position of the spectral amplitude peak in the pressure data records (Figures 2a, 3a and 3b). The cutoff frequency is in the 0.04–0.1 Hz range, thus providing source half duration in the 5–12.5 s range. By using the scaling relation between source half duration (τ in seconds) and seismic moment magnitude (M_0 in dyn.cm) (Ekström et al., 2012):

$$\tau = 1.05 \times 10^{-8} M_0 \quad (3)$$

we obtain an estimate of seismic moment magnitude (M_w) between 6.6 and 7.4 (real value is 7.3).

The pressure records allow us to pick S waves and maximum amplitude Rayleigh surface wave, at 14-s period, in the records of balloons 16 and 17. The differential time between these two phases is estimated to 86 and 209 s respectively for balloons 17 and 16, with an error bar of about 15 s. By using prior models of planet internal structure, we can estimate how this differential time is evolving with horizontal distance to the quake, and thus provide a distance estimate for these two balloons. Our modeling demonstrates that S waves propagate at about 4.2 km/s and seismic Rayleigh waves with a period of 14-s at about 2.9 km/s. Thus distance estimates are respectively 665–946 km and 1,817–2,099 km for balloons 17 and 16 (real values are 684 and 1,723 km). From these two distances, two potential surface locations can be provided.

A quake origin time can also be estimated assuming the velocity of surface waves (2.9 km/s) is properly estimated. The quake origin time is estimated to be 03:20:46 UTC \pm 50 s (real value is 03:20:36) from the arrival time of seismic Rayleigh waves at balloon 16.

Another important phenomenon linked to the planet internal structure is the dispersion of Rayleigh seismic surface waves. Figures 4b and 4c present scalograms of pressure records of balloon 16 (b) and vertical component of seismometer DAV (c) computed with a continuous wavelet transform using the Morse wavelet. The Morse wavelet is chosen because it is well localized in time/frequency domain, and because of its waveform similarity with the wave like signals expected here. The use of scalograms for time/frequency domain dispersion curve

analysis has already proven its efficiency on similar signals (Brissaud et al., 2021). This tool enhances the wave like patterns with dominant energy in the signal. While the dispersion is difficult to observe on balloon 17 due to the interference between various waves at short distance from the source, balloon 16 presents a record consistent with surface wave dispersion (Figure 4b). The dispersion of the fundamental mode of Rayleigh seismic surface waves is computed for an internal structure model described Table S1 in Supporting Information S1. This model is taking into account the local crustal structure extracted from CRUST2.0 model (Bassin, 2000) on top of AK135 global seismic model (Kennett et al., 1995). Rayleigh wave group velocities are computed from the phase velocity dispersion curves obtained by the Computer Programs in Seismology code (Herrmann, 2013). As shown in Figure 4b the predicted arrival times of the fundamental mode of Rayleigh seismic surface wave estimated from prior internal structure models, and distance and origin time estimated only from balloon data, properly reproduce the dispersion features observed on balloon pressure records.

A more precise evaluation of the internal structure model would require a joint inversion of S wave arrival time and Rayleigh wave dispersion curve to estimate both quake parameters (location and origin time) and planetary internal structure (Panning et al., 2015). However our simple analysis demonstrates that the balloon-borne pressure records can be used to estimate the quake magnitude within 0.8 units, the quake location within 300 km, and the quake origin time within 50 s. Moreover the Rayleigh wave dispersion curve observed on balloon records is consistent with internal structure models.

5. Conclusion

Unique balloon-borne observations of acoustic waves induced by quakes have allowed us to demonstrate that quake parameters and planetary internal structures can be inferred from balloon pressure data. These data also suggest that resonance modes of the balloon system must be taken into account, and that surface topography and/or resonances in the ground below the balloon can have a significant influence on the records. This first terrestrial demonstration of the capability of a balloon network to record and locate quakes is thus very encouraging for planetary applications, in particular for missions that target our sister planet Venus (Cutts et al., 2021; Izraelevitz et al., 2021). Moreover, the recording of infrasound from tectonic events on board balloons has potential applications similar to the ones already demonstrated for ground sensors, such as strong motion mapping in the quake source area (Shani-Kadmiel et al., 2021) or volcanic eruption monitoring (Marchetti et al., 2019). Finally, balloons may allow a rapid deployment of sensors after a seismic crisis (Brissaud et al., 2021) and, if combined with station keeping by maneuverable balloons (Bellemare et al., 2020), such a network of balloons may complement seismic networks above the source region.

Data Availability Statement

The TSEN pressure records and balloon GPS locations described in this study are available through this link at the following doi: <https://doi.org/10.5281/zenodo.6344454>. The seismic records used in this study were collected at IRIS data management center through the Wilber3 web interface: <https://ds.iris.edu/wilber3/>. The quake parameters were extracted from GlobalCMT data base: <https://www.globalcmt.org/CMTsearch.html>.

References

- Astafyeva, E. (2019). Ionospheric detection of natural hazards. *Reviews of Geophysics*, 57(4), 1265–1288. <https://doi.org/10.1029/2019rg000668>
- Bassin, C. (2000). The current limits of resolution for surface wave tomography in North America. *Eos, Transactions American Geophysical Union*, 81.
- Bellemare, M. G., Candido, S., Castro, P. S., Gong, J., Machado, M. C., Moitra, S., et al. (2020). Autonomous navigation of stratospheric balloons using reinforcement learning. *Nature*, 588(7836), 77–82. <https://doi.org/10.1038/s41586-020-2939-8>
- Bowman, D. C., & Krishnamoorthy, S. (2021). Infrasound from a buried chemical explosion recorded on a balloon in the lower stratosphere. *Geophysical Research Letters*, 48(21), e2021GL094861. <https://doi.org/10.1029/2021gl094861>
- Bowman, D. C., & Lees, J. M. (2018). Upper atmosphere heating from ocean-generated acoustic wave energy. *Geophysical Research Letters*, 45(10), 5144–5150. <https://doi.org/10.1029/2018GL077737>
- Brissaud, Q., Krishnamoorthy, S., Jackson, J. M., Bowman, D. C., Komjathy, A., Cutts, J. A., et al. (2021). The first detection of an earthquake from a balloon using its acoustic signature. *Geophysical Research Letters*, 48(12), e2021GL093013. <https://doi.org/10.1029/2021gl093013>
- Cutts, J. A., Krishnamoorthy, S., Jackson, J. M., Byrne, P. K., Komjathy, A., Pauken, M., et al. (2021). Balloon Infrasound Networks for Investigating the Venus Interior. In *52nd lunar and planetary science conference* (p. 2319).
- Eksröm, G., Nettles, M., & Dziewoński, A. (2012). The global CMT project 2004–2010: Centroid-moment tensors for 13, 017 earthquakes. *Physics of the Earth and Planetary Interiors*, 200–201, 1–9. <https://doi.org/10.1016/j.pepi.2012.04.002>

Acknowledgments

Centre National d'Etudes Spatiales supported this study through the development and operation of Strateole-2 balloon missions, and through the funding of associated Research Projects by both Atmosphere and Solar System divisions. Direction Générale de l'Armement supported authors affiliated to ISAE-SUPAERO. The authors thank Dany Bowman and an anonymous referee for improving this study through their reviews. We thank Naomi Murdoch for correcting the English language of this paper.

- Garcia, R. F., Bruinsma, S., Lognonné, P. H., Doornbos, E., & Cachoux, F. (2013). GOCE: The first seismometer in orbit around the Earth. *Geophysical Research Letters*, *40*(5), 1015–1020. <https://doi.org/10.1002/grl.50205>
- Garcia, R. F., Doornbos, E., Bruinsma, S., & Hebert, H. (2014). Atmospheric gravity waves due to the Tohoku-Oki tsunami observed in the thermosphere by GOCE. *Journal of Geophysical Research*, *119*(8), 4498–4506. <https://doi.org/10.1002/2013JD021120>
- Garcia, R. F., Lognonné, P. H., & Bonnin, X. (2005). Detecting atmospheric perturbations produced by Venus quakes. *Geophysical Research Letters*, *32*(16), 1–4. <https://doi.org/10.1029/2005GL023558>
- Garcia, R. F., Martire, L., Chaigneau, Y., Cadu, A., Mimoun, D., Portus, M. B., et al. (2020). An active source seismo-acoustic experiment using tethered balloons to validate instrument concepts and modelling tools for atmospheric seismology. *Geophysical Journal International*, *225*(1), 186–199. <https://doi.org/10.1093/gji/ggaa589>
- Haase, J., Alexander, M., Hertzog, A., Kalnajs, L., Deshler, T., Davis, S., et al. (2018). Around the world in 84 days. *Eos*, *99*. <https://doi.org/10.1029/2018eo091907>
- Herrmann, R. B. (2013). Computer programs in seismology: An evolving tool for instruction and research. *Seismological Research Letters*, *84*(6), 1081–1088. <https://doi.org/10.1785/0220110096>
- Hines, C. O. (1960). Internal atmospheric gravity waves at ionospheric heights. *Canadian Journal of Physics*, *38*(11), 1441–1481. <https://doi.org/10.1139/p60-150>
- Izraelievitz, J. S., Pauken, M., Krishnamoorthy, S., Goel, A., Aiazzi, C., Dorsky, L., et al. (2021). Hangar Flight Testing of a Subscale Venus Variable-Altitude Aerobot. In *19th meeting of the venus exploration analysis group (vexag)19th meeting of the venus exploration analysis group (vexag)* (Vol. 19, p. 8034).
- Kassarjian, E., Sanfedino, F., Alazard, D., Evain, H., & Montel, J. (2021). Modeling and stability of balloon-borne gondolas with coupled pendulum-torsion dynamics. *Aerospace Science and Technology*, *112*, 106607. <https://doi.org/10.1016/j.ast.2021.106607>
- Kennett, B. L., Engdahl, E., & Buland, R. (1995). Constraints on seismic velocities in the Earth from traveltimes. *Geophysical Journal International*, *122*(1), 108–124. <https://doi.org/10.1111/j.1365-246x.1995.tb03540.x>
- Krishnamoorthy, S., Lai, V. H., Komjathy, A., Pauken, M. T., Cutts, J. A., Garcia, R. F., et al. (2019). Aerial seismology using balloon-based barometers. In *IEEE transactions on geoscience and remote sensing* (Vol. 1–11). <https://doi.org/10.1109/TGRS.2019.2931831>
- Lognonné, P. H., Artru, J., Garcia, R. F., Crespon, F., Ducic, V., Jeansou, E., et al. (2006). Ground-based GPS imaging of ionospheric post-seismic signal. *Planetary and Space Science*, *54*(5), 528–540. <https://doi.org/10.1016/j.pss.2005.10.021>
- Marchetti, E., Lacanna, G., Pichon, A. L., Piccinini, D., & Ripepe, M. (2016). Evidence of large infrasonic radiation induced by earthquake interaction with alluvial sediments. *Seismological Research Letters*, *87*(3), 678–684. <https://doi.org/10.1785/0220150223>
- Marchetti, E., Ripepe, M., Campus, P., Le Pichon, A., Vergoz, J., Lacanna, G., et al. (2019). Long range infrasound monitoring of Etna volcano. *Scientific Reports*, *9*(1), 18015. <https://doi.org/10.1038/s41598-019-54468-5>
- Martire, L., Brissaud, Q., Lai, V. H., Garcia, R. F., Martin, R., Krishnamoorthy, S., et al. (2018). Numerical simulation of the atmospheric signature of artificial and natural seismic events. *Geophysical Research Letters*, *45*(21), 12085–12093. <https://doi.org/10.1029/2018GL080485>
- Martire, L., Martin, R., Brissaud, Q., & Garcia, R. F. (2022). SPECSEM2d-DG, an open-source software modelling mechanical waves in coupled solid–fluid systems: The linearized Navier–Stokes approach. *Geophysical Journal International*, *228*(1), 664–697. <https://doi.org/10.1093/gji/ggab308>
- Mutschlechner, J. P., & Whitaker, R. W. (2005). Infrasound from earthquakes. *Journal of Geophysical Research*, *110*(D1), D01108. <https://doi.org/10.1029/2004JD005067>
- Panning, M. P., Beucler, É., Drilleau, M., Mocquet, A., Lognonné, P., & Banerdt, W. B. (2015). Verifying single-station seismic approaches using Earth-based data: Preparation for data return from the InSight mission to Mars. *Icarus*, *248*, 230–242. <https://doi.org/10.1016/j.icarus.2014.10.035>
- Pichon, A. L., Mialle, P., Guilbert, J., & Vergoz, J. (2006). Multistation infrasonic observations of the Chilean earthquake of 2005 June 13. *Geophysical Journal International*, *167*(2), 838–844. <https://doi.org/10.1111/j.1365-246x.2006.03190.x>
- Podglajen, A., Hertzog, A., Plougonven, R., & Žagar, N. (2014). Assessment of the accuracy of (re) analyses in the equatorial lower stratosphere. *Journal of Geophysical Research: Atmospheres*, *119*(19), 11–166. <https://doi.org/10.1002/2014JD021849>
- Salomons, E. M. (2001). *Computational atmospheric acoustics*. Springer Science & Business Media.
- Shani-Kadmiel, S., Assink, J. D., Smets, P. S. M., & Evers, L. G. (2018). Seismoacoustic coupled signals from earthquakes in central Italy: Epicentral and secondary sources of infrasound. *Geophysical Research Letters*, *45*(1), 427–435. <https://doi.org/10.1002/2017gl076125>
- Shani-Kadmiel, S., Averbuch, G., Smets, P., Assink, J., & Evers, L. (2021). The 2010 Haiti earthquake revisited: An acoustic intensity map from remote atmospheric infrasound observations. *Earth and Planetary Science Letters*, *560*, 116795. <https://doi.org/10.1016/j.epsl.2021.116795>
- Stevenson, D., Cutts, J. A., & Mimoun, D. (2015). *Probing the interior structure of Venus*. (Tech. Rep.). Keck Institute for Space Studies.
- Vincent, R. A., & Hertzog, A. (2014). The response of superpressure balloons to gravity wave motions. *Atmospheric Measurement Techniques*, *7*(4), 1043–1055. <https://doi.org/10.5194/amt-7-1043-2014>
- Waxler, R., & Assink, J. (2019). Propagation modeling through realistic atmosphere and benchmarking. In *Infrasound monitoring for atmospheric studies* (pp. 509–549). Springer. https://doi.org/10.1007/978-3-319-75140-5_15